





## Article

# Effect of Ion Selectivity on Current Production in Sewage Microbial Fuel Cell Separators

Ryoya Itoshiro <sup>1,†</sup>, Naoko Yoshida <sup>1,\*</sup>,, Toshiyuki Yagi <sup>1</sup>, Yuriko Kakihana <sup>2</sup> and Mitsuru Higa <sup>2</sup>

<sup>1</sup> Department of Civil Engineering, Nagoya Institute of Technology (Nitech), Nagoya 466-8555, Japan; r.itoshiro.994@stn.nitech.ac.jp (R.I.); yagi.toshiyuki@nitech.ac.jp (T.Y.)

<sup>2</sup> Graduate School of Sciences and Technology for Innovation, Yamaguchi University, Yoshida, Yamaguchi 753-8511, Japan; kakihana@yamaguchi-u.ac.jp (Y.K.); mhiga@yamaguchi-u.ac.jp (M.H.)

\* Correspondence: yoshida.naoko@nitech.ac.jp; Tel.: +81-527-895-437

† These authors contributed equally to this study.

**Abstract:** This study compared the performance of two microbial fuel cells (MFCs) equipped with separators of anion or cation exchange membranes (AEMs or CEMs) for sewage wastewater treatment. Under chemostat feeding of sewage wastewater (hydraulic retention time of approximately 7 h and polarization via an external resistance of 1  $\Omega$ ), the MFCs with AEM (MFC<sub>AEM</sub>) generated a maximum current that was 4–5 times greater than that generated by the MFC with CEM (MFC<sub>CEM</sub>). The high current in the MFC<sub>AEM</sub> was attributed to the approximately neutral pH of its cathode, in contrast to the extremely high pH of the MFC<sub>CEM</sub> cathode. Due to the elimination of the pH imbalance, the cathode resistance for the MFC<sub>AEM</sub> (13–19  $\Omega \cdot m^2$ ) was lower than that for the MFC<sub>CEM</sub> (41–44  $\Omega \cdot m^2$ ). The membrane resistance measured as the Cl<sup>-</sup> mobility of AEMs for the MFC<sub>AEM</sub> operated for 35, 583, and 768 days showed an increase with operation time and depth, and this increase contributed minimally to the cathode resistance of the MFC<sub>AEM</sub>. These results indicate the advantage of the AEM over the CEM for air-cathode MFCs. The membrane resistance may increase when the AEM is applied in large-scale MFCs on a meter scale for extended periods.

**Keywords:** microbial fuel cell; wastewater treatment; anion exchange membrane; cation exchange membrane; membrane resistance



**Citation:** Itoshiro, R.; Yoshida, N.; Yagi, T.; Kakihana, Y.; Higa, M. Effect of Ion Selectivity on Current Production in Sewage Microbial Fuel Cell Separators. *Membranes* **2022**, *12*, 183. <https://doi.org/10.3390/membranes12020183>

Academic Editors: August Bonmati and Miriam Cerrillo

Received: 30 November 2021

Accepted: 31 January 2022

Published: 3 February 2022

**Publisher's Note:** MDPI stays neutral with regard to jurisdictional claims in published maps and institutional affiliations.



**Copyright:** © 2022 by the authors. Licensee MDPI, Basel, Switzerland. This article is an open access article distributed under the terms and conditions of the Creative Commons Attribution (CC BY) license (<https://creativecommons.org/licenses/by/4.0/>).

## 1. Introduction

Wastewater treatment is becoming extremely important in present times. It is crucial not only in conserving public water quality but also in supplying sufficient quantities of safe water to address rapidly increasing demands [1]. Water treatment technology is widely used. However, electricity consumption in sewage treatment accounts for 0.7–4% of domestic electricity consumption in developed countries [2,3], and a substantial amount of greenhouse gases are emitted. To ensure sustainable water cycles, the wastewater treatment should maximize energy conservation by recovering the biomass energy contained in wastewater [4]. Typically, most of the energy recovered is obtained from converting sludge biomass into biogas [4] via microbial fermentation and solid fuel [5]. However, because of the low biomass concentration and substantial volume of wastewater, energy recovery from wastewater is still in the research stage. Several treatment methods that integrate energy recovery, such as microalgae cultivation, membrane-enriched fermentation, and microbial fuel cells (MFCs) [6], have been evaluated in the past. Among these, MFCs received the most attention for treating wastewater with simultaneous recovery of electricity [7].

MFCs generally comprise an anode, a cathode, and a separator. The anode collects electrons that are emitted by the microbial oxidization of organic matter in an anolyte, such as wastewater. The cathode reduces oxidants such as oxygen using electrons collected in the anode. The separator insulates the electrodes while maintaining the mobility of the ions or oxidants. Air-cathode MFCs are the most common type of MFCs and have a single

anolyte chamber with cathodes exposed to the air. The catalysts for the anode reactions are microorganisms that degrade various organic matter, and the catalysts for cathode reactions are carbon particles that can reduce oxygen. Currently, the limited electric power production of the MFCs makes them impractical for application in real wastewater treatment. The performance of all three key components needs to be improved [8], particularly in terms of scaling-up. The challenges include developing (i) low-cost mass production technology for the anode, (ii) improved oxygen reducing catalyst for the cathode, and (iii) a resilient separator with high ion mobility. Among them, the selection of the separator significantly affects the performance of the MFC and the lifetime required to generate electric power.

The first air-cathode MFCs were equipped with proton-exchange [9] and later equipped with ion-exchange membranes (IEMs) because of cost effectiveness. Both membranes have been extensively used in hydrogen fuel cells [10] and iron-based flow-battery systems [11]. Non-ion-exchange membranes (NIEs) have been used as separators [12–15] in combination with polytetrafluoroethylene (PTFE) gas diffusion layers (GDLs), which have oxygen mobility [16]. Examples of such membranes include glass fiber mats, polypropylene porous plastic plates, and non-woven fabrics. Compared to IEMs, systems with GDL and NIEs enable lower costs, although the cathode facing the liquid phase generally has a short lifetime due to biofouling on the cathode [17]. The MFCs with GDLs and NIEs exhibited a 34% decrease in electricity production after one month [13]; washing was required to recover the initial levels of performance [18,19] that was caused by aerobic bacterial growth on the cathode facing the wastewater. In contrast, the MFCs equipped with a cation exchange membrane (CEM) performed almost consistently over an entire year [20,21]. Recently, a scalable air-cathode MFCs equipped with an anion exchange membrane (AEM) was demonstrated for the first time [2], and electricity was successfully recovered from sewage wastewater over a year [22]. A comparison of electric power production by MFCs using AEMs and CEMs demonstrated the advantage of AEMs, which mitigate the pH imbalances that are often observed in MFCs with CEMs [23–25]. However, comparative studies are limited to milliliter scales in batch mode, making it difficult to evaluate the effects on the performance of MFCs in actual wastewater treatment.

In this study, the effect of the ion selectivity of IEMs on MFCs performance was evaluated in air-cathode MFCs equipped with AEMs and CEMs. These MFCs were operated in the chemostat in a sewage wastewater treatment plant, and the electric power density, chemical oxygen demand (COD) removal efficiency (COD-RE), membrane resistance, and cathode resistance were compared. In addition, the effect of operation time on the AEM resistance was evaluated to estimate the lifetime of the AEMs in the air cathode-MFC.

## 2. Materials and Methods

### 2.1. MFC Used in the Experiment

In this study, a cylindrical MFC core ( $\Phi 5 \text{ cm} \times 100 \text{ cm}$ ) with an air cathode [26] prepared from a stainless-steel mesh surrounded by a carbon-based cathode was used along with an IEMs and nonwoven graphite fabric (TOYOBO Co., Ltd., Osaka, Japan). The IEMs were either CEMs (CSE; Astom Co., Ltd., Tokyo, Japan) or AEMs (ASE; Astom Co., Ltd.). The thicknesses of the CEM and AEM were 0.16 and 0.15 mm, respectively. The membrane resistances were 0.18 and 0.26  $\Omega \cdot \text{m}^2$ , respectively, in 0.5 N NaCl at 25 °C according to the manufacturer's catalogue. Carbon cloths painted with a mixture of activated carbon and carbon black were used as cathodes. Twelve carbon brushes ( $\Phi 4.0 \text{ cm} \times 100 \text{ cm}$ ) were placed around the MFC core, in addition to the nonwoven graphite fabric. The MFC units of the core and 12 additional carbon brushes were defined as the MFC<sub>AEM</sub> and MFC<sub>CEM</sub> equipped with an AEM and a CEM as separators, respectively. A mixture of poly(diallyldimethylammonium chloride) (PDDMAC) and PTFE [2] were used as the binders of the carbon catalyst pastes for the MFC<sub>AEM</sub> and a 7 L/mg-mixture of carbon in a 10% Nafion solution were used for the MFC<sub>CEM</sub>, respectively. Carbon brushes were manufactured using carbon fabrics (T300B-3k-40B, Toray, Tokyo, Japan), soaked in acetone, and heated at

450 °C for 5 h before use [27] to render the surface sufficiently hydrophilic for microbial adhesion [28].

## 2.2. Operation of the MFC Reactors

The MFC<sub>AEM</sub> and MFC<sub>CEM</sub> were installed in cylindrical reactors (Φ25 cm × 110 cm) made of polyvinyl chloride and filled with 50 L of wastewater. The reactor was operated in a sewage wastewater treatment plant (Nagoya City) and continuously supplied with influent using a tubing pump (TP-20SA, AS ONE, Osaka, Japan) with a hydraulic retention time (HRT) of 2.6–9.8 h. The HRTs were set by changing the inflow rate to realize different COD concentrations in the reactor. For the initial 35 days, the influent of the primary sedimentation tank (PST) was used; later the effluent of the PST was used due to the clogging of the tube by the influent. Wastewater in the reactor was circulated at a circulation time of 15 min using a submersible pump (LEDGLE, Shenzhen, China). The cathode and anode of the MFC were connected via an external resistor ( $R_{ext}$ ) of 1 Ω and a voltage data logger (VR-71; T&D Co., Nagano, Japan) parallel to  $R_{ext}$ . The cell voltage between anode and cathode was recorded hourly.

## 2.3. Power Density Curve

Power density curves were measured for the MFC<sub>AEM</sub> and MFC<sub>CEM</sub> with HRTs of 3.0–9.8 h at 9, 18, and 30 days after the commencement of operation. As noted previously, the MFCs were connected in parallel with 1, 2, 5, 10, 20, 50, 100, and 10,000 Ω  $R_{ext}$  [29]. An Ag/AgCl reference electrode (RE-1B; BAS Co., Ltd., Tokyo, Japan) was installed close to the MFC anode, and the anode and cathode potentials were measured. The anode ( $R_{an}$ ) and cathode ( $R_{ca}$ ) resistances of the MFC were calculated by dividing the electrode potential difference by the current and multiplying it with the separator area [30].

## 2.4. COD Removal and Coulombic Efficiencies

COD was determined by adding potassium dichromate as an oxidizing agent and mercury as a reducing agent to the sample, followed by heating. Subsequently, the absorbance was measured with a spectrophotometer to determine the concentration [31]. The COD-RE [%] was calculated using Equation (1) with  $COD_{IN}$  [mg/L] and  $COD_{EF}$  [mg/L] values, that is, the concentrations of organic matter in the influent and effluent, respectively.

$$COD-RE = \frac{COD_{IN} - COD_{EF}}{COD_{IN}} \times 100. \quad (1)$$

Coulombic efficiency (CE) is the ratio of charge recovered as current to the total charge obtained from the decomposition of organic matter in sewage. It can be expressed by Equation (2).

$$CE = \frac{C_p}{C_T} \times 100. \quad (2)$$

where  $C_p$  [C] is the cumulative charge carried by the current during the given HRT and  $C_T$  [C] is the theoretical charge that is calculated using Equation (3).

$$C_T = \frac{\Delta COD \cdot V F b}{M}. \quad (3)$$

where  $\Delta C$  [g/L] is the difference between  $COD_{IN}$  and  $COD_{EF}$ ,  $V$  [L] is the volume of wastewater in the reactor,  $F$  [C/mol] is Faraday constant (=96,485 C/mol),  $b$  is number of moles of electrons produced from 1 mol of oxygen ( $b = 4$ ), and  $M$  [g/mol] is molecular weight of oxygen ( $M = 32$ ). The CE was determined by least-squares fitting of the measured and calculated currents using the CE as a variable in Equation (2).

## 2.5. Measuring Membrane Resistance

The electrical resistance of the AEM before and after 35, 583, and 768 days of operation was measured using a custom-built acrylic cell, as described in a previous study [32]. The

old AEMs (583 and 783 d) were taken from an air-cathode MFC [22] similar to the MFC used in this study. The AEMs were taken from the top, middle, and bottom of the cell, and cut into squares of approximately  $5\text{ cm} \times 5\text{ cm}$  (with an effective area of  $11\text{ cm}^2$ ). Following this, the cell was filled with a  $0.5\text{ M NaCl}$  solution. Two parallel Pt electrodes were placed on both sides of the AEM and connected to an LCR meter (AD-5827; A&D Co., Ltd., Tokyo, Japan). The membrane resistance ( $R_m$ ) [ $\Omega \cdot \text{cm}^2$ ] was calculated using the values of resistance measured between the electrodes with and without membranes, denoted by  $R_1$  and  $R_0$ , respectively, using the equation  $R_m = R_1 - R_0$ . The resistances were measured using alternating current (AC) at a frequency of  $10\text{ kHz}$ . It must also be noted that certain membranes were pre-incubated in  $0.5\text{ M NaCl}$ .

### 2.6. Linear Sweep Voltammetry (LSV) Test

The effect of the AEM ages on the cathode reaction was evaluated by monitoring the current in a small cylindrical reactor ( $\Phi 6\text{ cm} \times 5\text{ cm}$ ) equipped with  $0.5\text{ mg/cm}^2$  Pt-loaded carbon cloth [33] as the anode to avoid the restriction of the anode reaction, which is often observed in MFCs with low COD accessibility (Supplementary Figure S1). After operation for 35, 583, and 768 days, the cathodes and AEMs were set with the anode. The cathode and anode were used as the working electrode (WE) and counter electrode, respectively, and an Ag/AgCl reference electrode (012167RE-1B; BAS Co., Ltd., Tokyo, Japan) was placed near the anode. LSV measurements were performed using an electrochemical workstation (VMP-3; Bio-Logic, Claix, France) supplemented with hydrogen in the anolyte at approximately  $0.1\text{ MPa}$ . The WE potential was set to  $0.5\text{ V}$  and swept to  $-0.5\text{ V}$  vs. Ag/AgCl at  $0.5\text{ mV/s}$ .

### 2.7. Investigation of Dirt on Membrane

White precipitates on  $25\text{ cm}^2$  of the AEM (583 d) or CEM (35 d) were scrubbed and dissolved in  $10\text{ mL}$  of  $0.1\text{ N HCl}$ . The extracts were then filtered using a PTFE membrane filter ( $0.45\text{ }\mu\text{m}$  pore size) (Merck Millipore, Darmstadt, Germany). The filtrates were diluted 5–20 times and analyzed using an ion chromatography system (Shimadzu, Kyoto, Japan), including an electron conductivity detector (CDD-10Avp). Anions and cations in the samples were separated at  $40\text{ }^\circ\text{C}$  using Shim-pack IC-A3 ( $\Phi 4.6 \times 150\text{ mm}$ ) and Shim-pack IC-C4 ( $\Phi 4.6 \times 150\text{ mm}$ ), respectively. The mobile phase was a mixture of  $8\text{ mM}$  p-hydroxybenzoic acid,  $3.2\text{ mM}$  Bis-Tris, and  $50\text{ mM}$  boric acid for anion analysis and a mixture of  $2.5\text{ mM}$  oxalic acid dihydrate and  $5\text{ mM}$  18-Crown-6 for cation analysis.

The anode side of the AEM and CEM were observed by fluorescence microscopy after staining with SYBR Green II, a DNA-binding dye, as described in a previous study [34].

## 3. Results and Discussion

### 3.1. Current Production by the Two MFCs throughout the Operation

The  $\text{MFC}_{\text{AEM}}$  and  $\text{MFC}_{\text{CEM}}$  produced  $0.80\text{--}1.30\text{ A/m}^2$  of current with the PST influent, although the operation was terminated due to the frequent clogging in the influent tube. The  $\text{MFC}_{\text{AEM}}$  produced a current of  $0.30\text{--}0.70\text{ A/m}^2$  with a continuous inflow of the PST effluent for  $2.6\text{--}9.8\text{ h}$  of HRT. This current was approximately 4–5 times higher than that of  $\text{MFC}_{\text{CEM}}$ , which produced  $0.10\text{--}0.20\text{ A/m}^2$  (Figure 1). After 44 d, both  $\text{MFC}_{\text{AEM}}$  and  $\text{MFC}_{\text{CEM}}$  exhibited relatively stable currents, except for decreased currents in the  $\text{MFC}_{\text{AEM}}$  reactor due to pumping problems. The slightly lower current observed from days 60 to 70 was probably caused by the supplementation of low COD because of the dilution of the inflow by rainwater. Assuming similar anode resistances in the  $\text{MFC}_{\text{AEM}}$  and  $\text{MFC}_{\text{CEM}}$ , the difference in current production can be attributed to the cathode reaction, which is typically regulated by the oxygen reduction rate of the cathode catalyst, oxygen availability, and ion mobility. The membrane resistance determined by ion mobility was smaller in CEM ( $0.16\Omega \cdot \text{m}^2$ ) than in AEM ( $0.26\Omega \cdot \text{m}^2$ ) according to the manufacturer's catalogue. Both MFCs had identical loaded cathode catalyst and oxygen availability. However, they had different binder components, that is, a mixture of PDDMAC and PTFE for  $\text{MFC}_{\text{AEM}}$ , and



Nafion for  $MFC_{CEM}$ , which could potentially cause differences in oxygen availability to the carbon catalyst. Another factor was the difference in pH at the cathode. An approximate pH of 10–11 was measured on the cathode surface with CEM, in contrast to a neutral pH on that with AEM. This pH imbalance restricts electron transfer to oxygen, as suggested in a previous study [25]. Collectively, the differences in ion mobility, binder components, and pH resulted in higher current production in the  $MFC_{AEM}$ .

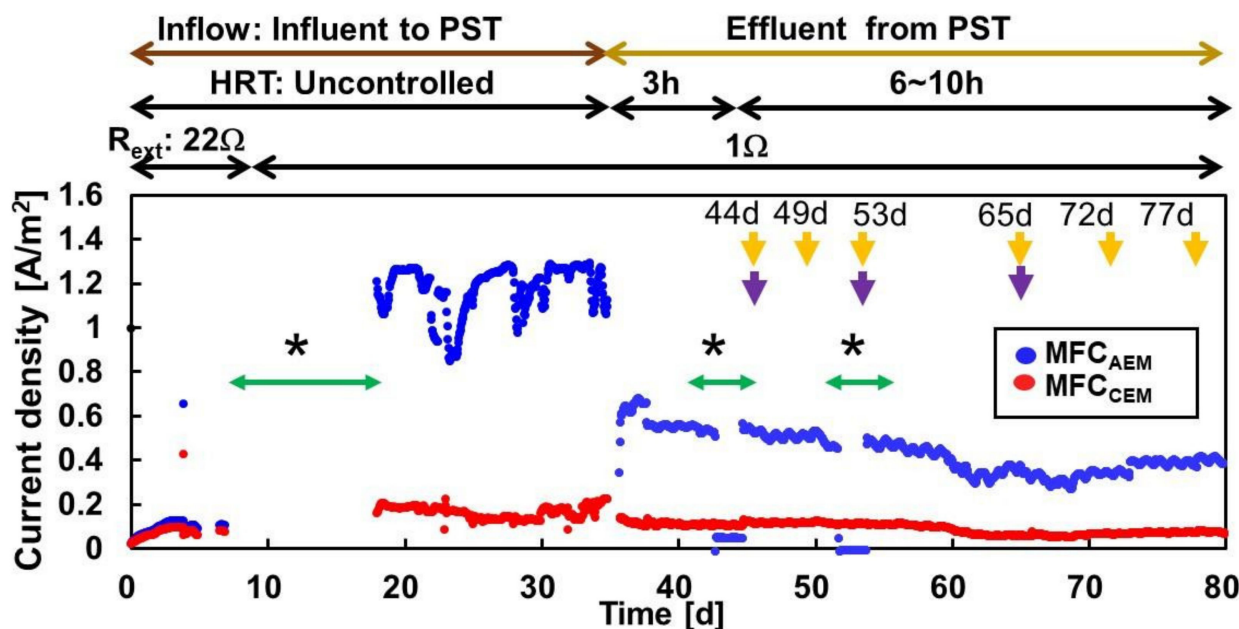


**Figure 1.** Current production by  $MFC_{AEM}$  and  $MFC_{CEM}$  throughout the operation. \* Indicates the times when the data logger had trouble with the MFC. Purple and yellow arrows indicate the timing for PI curve or COD analysis, respectively.

The current density was similar to that generated by a similar MFC core without carbon brushes. The MFC without carbon brushes was also operated in the PST effluent with continuous inflow for 6 h of HRT using  $2\ \Omega$  of the external resistance and recorded an average current density of  $0.32\ \text{A}/\text{m}^2$  [26]. The  $MFC_{AEM}$  used in this study produced an average of  $0.38\ \text{A}/\text{m}^2$  for 6 h of HRT. This was unexpected because the increase in the anodic area caused by introducing the carbon brushes has been demonstrated in several studies [35,36]. The similarity in current production, despite the increase in the anodic area, was due to the reaction restriction of the cathode.

### 3.2. COD Removal and CE

The  $\text{COD}_{IN}$  for the two MFCs was  $210 \pm 40\ \text{mg}/\text{L}$ . MFC treatment at  $\text{HRT} = 7\ \text{h}$  resulted in  $66 \pm 9.0\ \text{mg}/\text{L}$  and  $99 \pm 51\ \text{mg}/\text{L}$  of  $\text{COD}_{EF}$  for the  $MFC_{AEM}$  and  $MFC_{CEM}$ , respectively (Table 1). The COD-REs of  $MFC_{AEM}$  and  $MFC_{CEM}$  were  $69\% \pm 2.0\%$  and  $54\% \pm 19\%$ , respectively, and were not significantly different ( $p > 0.05$ ). The CEs of  $MFC_{AEM}$  and  $MFC_{CEM}$  were  $1.6 \pm 0.40\%$  and  $0.50 \pm 0.35\%$ , respectively. The superiority of  $MFC_{AEM}$  in current recovery indicates the higher CE in  $MFC_{AEM}$  than in  $MFC_{CEM}$ .

The COD-RE achieved in the MFC indicated an improvement compared to that obtained with our previous  $MFC_{AEM}$ , which exhibited 30% COD-RE at  $\text{HRT} = 6\ \text{h}$  [26]; the COD-RE increased by approximately twice upon the introduction of carbon brushes. In addition, the CE was drastically reduced to less than 10% of that of the previous MFC without carbon brushes (23%) due to the reduction in specific cathode or separator areas with respect to wastewater volume; the introduction of 12 carbon brushes reduced the specific area from  $14\ \text{m}^2/\text{m}^3$  [26] to  $3.2\ \text{m}^2/\text{m}^3$  in this study. These results indicate the importance of determining the optimum ratio of carbon brushes to a specific cathode

area [37]. However, the optimum ratio of carbon brushes to the  $MFC_{AEM}$  is expected to vary at different CODs in the MFC reactor. This necessitates comprehensive MFC performance modeling that integrates COD as well as the anode and cathode surface areas.

**Table 1.** Summary of operation conditions of the  $MFC_{AEM}$  and  $MFC_{CEM}$  and the resulting performances in COD-RE, CE, OCV,  $I_{max}$ , and  $P_{max}$ .

	IEM Type	Operation Time						Average (49, 72, 77 d)
		44 d	53 d	65 d	49 d	72 d	77 d	
HRT [h]	AEM	3.3	6.9	9.8	6.4	7.6	7.3	$7.1 \pm 0.7$
	CEM	3.0	6.9	8.8	6.9	7.3	7.3	$7.2 \pm 0.3$
COD <sub>IN</sub> [mg/L]	AEM	-	-	-	230	230	170	$210 \pm 40$
	CEM	-	-	-	230	230	170	$210 \pm 40$
COD <sub>EF</sub> [mg/L]	AEM	-	-	-	73	69	57	$66 \pm 9.0$
	CEM	-	-	-	150	76	70	$99 \pm 51$
COD-RE [%]	AEM	-	-	-	68	70	67	$69 \pm 2.0$
	CEM	-	-	-	35	67	59	$54 \pm 19$
CE [%]	AEM	-	-	-	1.7	1.2	1.8	$1.6 \pm 0.4$
	CEM	-	-	-	0.85	0.27	0.46	$0.50 \pm 0.35$
OCV [V]	AEM	0.43	0.37	0.39	-	-	-	-
	CEM	0.26	0.26	0.25	-	-	-	-
$I_{max}$ [A/m <sup>2</sup> ]	AEM	0.59	0.49	0.33	-	-	-	-
	CEM	0.13	0.11	0.089	-	-	-	-
$P_{max}$ [W/m <sup>2</sup> ]	AEM	0.064	0.047	0.032	-	-	-	-
	CEM	0.0081	0.0075	0.0037	-	-	-	-

### 3.3. Polarization Curve

Figure 2 shows the polarization curves for the  $MFC_{AEM}$  and  $MFC_{CEM}$  at HRTs in the range of 3.0–9.8 h. The open-circuit voltage (OCV) of the  $MFC_{AEM}$  was the highest (0.43 V) for an HRT of 3.3 h and decreased to 0.37 and 0.39 V for an HRT of 6.9 and 9.8 h (Figure 2B, Table 1), respectively. The maximum power density ( $P_{max}$ ) showed a similar trend and was 0.064 W/m<sup>2</sup> for an HRT of 3.3 h and decreased to 0.047 W/m<sup>2</sup> and 0.032 W/m<sup>2</sup> at 6.9 h and 9.8 h, respectively. The maximum current density ( $I_{max}$ ) decreased marginally with the increase in HRT; it was 0.59 A/m<sup>2</sup> at 3.0 h and decreased to 0.49 A/m<sup>2</sup> and 0.33 A/m<sup>2</sup> at 6.9 h and 9.8 h, respectively. The HRT-dependent decrease in electricity generation has been repeatedly observed in the MFC in previous studies [2,22,26]. This decrease was revealed by the low COD due to the extended time required for microbial degradation.

The  $MFC_{CEM}$  had an OCV of 0.25–0.26 V,  $I_{max}$  of 0.089–0.13 A/m<sup>2</sup>, and  $P_{max}$  of 0.0037–0.0081 W/m<sup>2</sup>, regardless of the HRT (Figure 2A,B, Table 1). The OCV,  $I_{max}$ , and  $P_{max}$  for the  $MFC_{CEM}$  were 60–70%, 22–26%, and 12–16% those of  $MFC_{AEM}$  at similar HRTs, respectively. The stable but lower OCV,  $I_{max}$ , and  $P_{max}$  in the  $MFC_{CEM}$  indicates a limitation of the cathode reaction rate in the  $MFC_{CEM}$  because of the pH imbalance in the  $MFC_{CEM}$  [25].

The differences in the resistance between the  $MFC_{AEM}$  and  $MFC_{CEM}$  were considered by dividing the resistances by the anode ( $R_{an}$ ) and cathode ( $R_{ca}$ ) resistances. The  $R_{an}$  values of the  $MFC_{AEM}$  were 3.2, 3.4, and 6.9 mΩ·m<sup>2</sup> at 3.3, 6.9, and 9.8 h, respectively. These values indicated that the COD accessibility in the anolyte affected the  $R_{an}$  (Figure 2D, Table 2). The  $R_{an}$  of the  $MFC_{CEM}$  was 1.7–1.9 mΩ·m<sup>2</sup> and lower than that of the  $MFC_{AEM}$ . In contrast, the  $R_{ca}$  of  $MFC_{AEM}$  was 13–19 mΩ·m<sup>2</sup> and approximately 27–43% that of the  $MFC_{CEM}$  (41–49 mΩ·m<sup>2</sup>). These results indicated that the higher electricity production in the  $MFC_{AEM}$  can be attributed to the lower  $R_{ca}$  in the  $MFC_{AEM}$  (Figure 2C, Table 2).

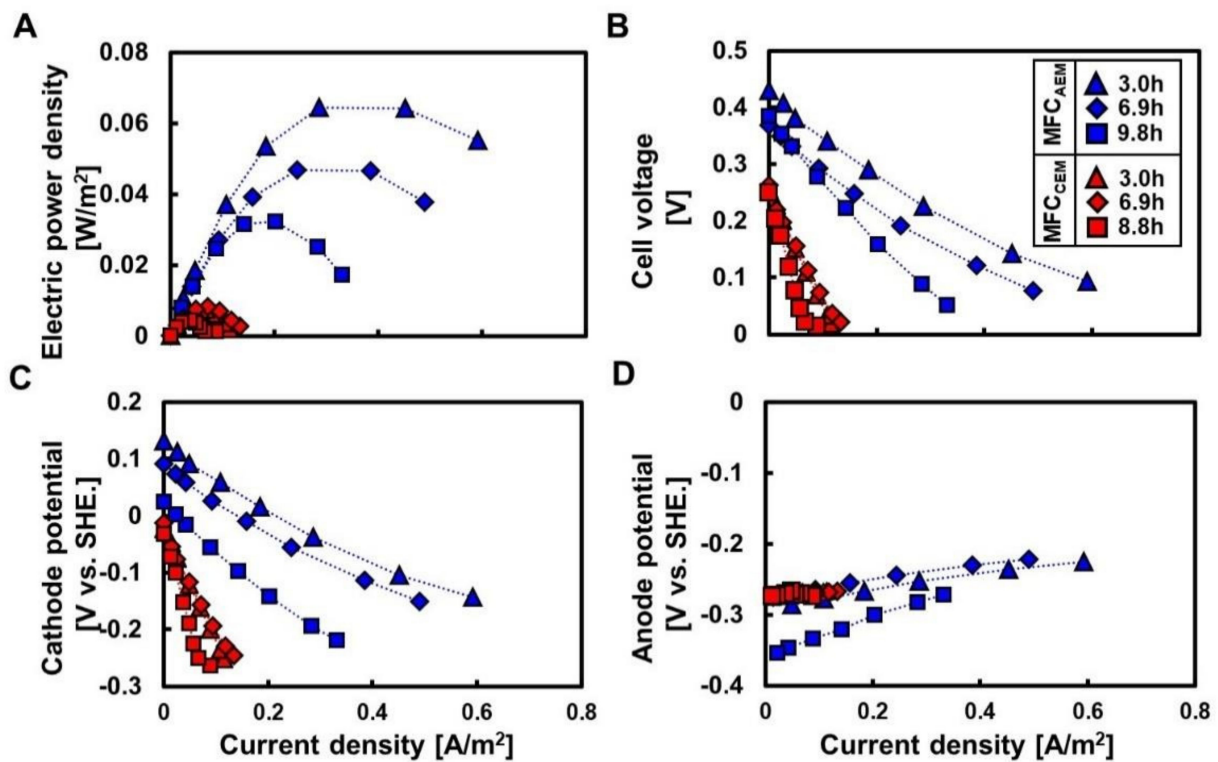


**Figure 2.** Effects of ion selectivity of the membrane separator on electricity and potential. Panels (A,B) present power density (A) and cell voltage (B) with varied currents, respectively. Panels (C,D) present cathode (C) and anode potential (D) at different current densities, respectively.

**Table 2.** Summary of resistance measured in this study.

Time (d)	Depth [cm]	R <sub>an</sub> -MFC <sub>CEM</sub> [mΩ·m <sup>2</sup> ]	R <sub>ca</sub> -MFC <sub>CEM</sub> [mΩ·m <sup>2</sup> ]	R <sub>an</sub> -MFC <sub>AEM</sub> [mΩ·m <sup>2</sup> ]	R <sub>ca</sub> -MFC <sub>AEM</sub> [mΩ·m <sup>2</sup> ]	R <sub>ca</sub> -H <sub>2</sub> [mΩ·m <sup>2</sup> ]	R <sub>M-Cl</sub> [mΩ·m <sup>2</sup> ]	R <sub>M-Cl</sub> * [mΩ·m <sup>2</sup> ]
0						6.7	0.31	-
44		1.8	41	3.2	13		-	-
53		1.9	49	3.4	13		-	-
65		1.7	44	6.9	19		-	-
35	20						0.34	0.32
35	50					10	0.36	0.30
35	80						0.38	0.29
583	20						0.27	0.22
583	50					7.5	0.37	0.28
583	80						0.53	0.39
768	50					7.7	0.61	0.32

Depth: depth from the water surface [cm]; R<sub>an</sub>: anode resistance of the MFC; R<sub>ca</sub>: cathode resistance of the MFC; R<sub>ca-H<sub>2</sub></sub>: cathode resistance of the H<sub>2</sub> oxidizing fuel cell; R<sub>M-Cl</sub>: membrane resistance; \* R<sub>M-Cl</sub> measured after immersion for 6 weeks.

The I<sub>max</sub> and P<sub>max</sub> of the MFC<sub>AEM</sub> were in the ranges observed in our previous study without carbon brushes and with 91 mg/L of COD [22], that is, 0.19–0.38 A/m<sup>2</sup> and 0.038–0.081 W/m<sup>2</sup>, respectively. The enhancement of the carbon brushes was restricted due to the low COD and limitation of the cathode reaction in the MFC<sub>AEM</sub>.

According to the results presented in Sections 3.1–3.3, the superiority of the AEM as a separator in an air-cathode MFC was apparent. Therefore, the resistance of the cathode in MFC<sub>AEM</sub> was further investigated.

### 3.4. Linear Sweep Voltammetry

The color change of the AEM from clear to dark brown (Figure 3) after extended operation of the MFC<sub>AEM</sub> [22], motivated us to evaluate the effect of operation time on current production by the MFC<sub>AEM</sub>. The surface apparatus differed on either side of the AEM; the anode side was covered with a dark brown film, whereas the cathode side was covered with white precipitates. The effect of dirt on the current production was evaluated by LSV.

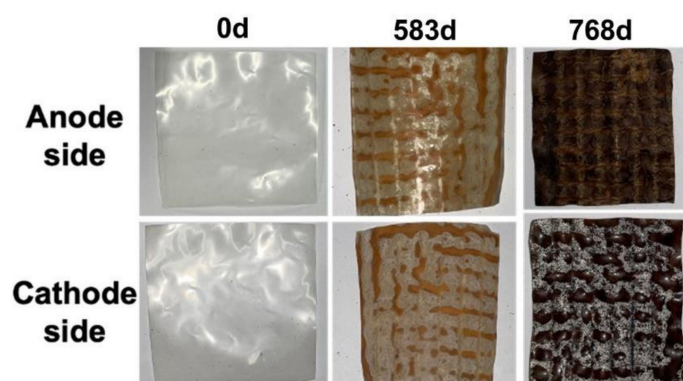


Figure 3. Change in AEM appearance with operation age.

The LSV was performed using a small air-cathode fuel cell filled with sewage wastewater and using Pt as the anode catalyst under H<sub>2</sub> supplementation to prevent the restriction of the microbial anode reaction (Supplementary Figure S1). The original AEM (AEM<sub>0</sub>) and AEMs (AEM<sub>35</sub>, AEM<sub>583</sub>, and AEM<sub>768</sub>) taken from the MFC<sub>AEM</sub> after 35, 583, and 768 days of operation exhibited a marginal increase in the slope, i.e., the cathode resistance ( $R_{ca-H_2}$ ), with the increase in operation time (Figure 4). The  $R_{ca-H_2}$  for all AEMs remained apparently unchanged at  $8.0 \pm 2.0 \text{ m}\Omega \cdot \text{m}^2$  (Figure 4, Table 2). A similar  $R_{ca-H_2}$  indicates a minor effect of dirt on the cathode resistance. The potential of the cells with AEM<sub>583</sub> and AEM<sub>768</sub> was marginally higher than that of AEM<sub>0</sub> and AEM<sub>35</sub>, although the mechanism behind it is unknown.

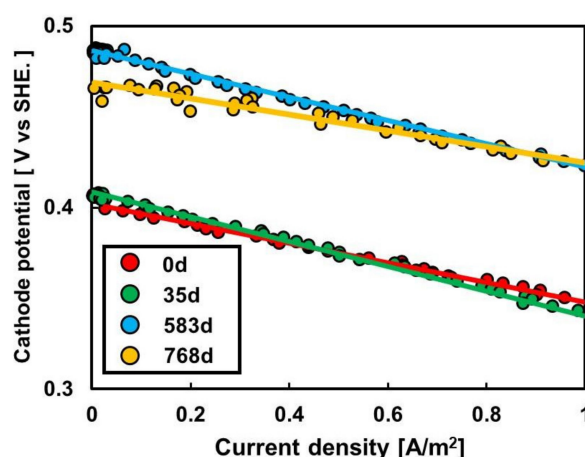
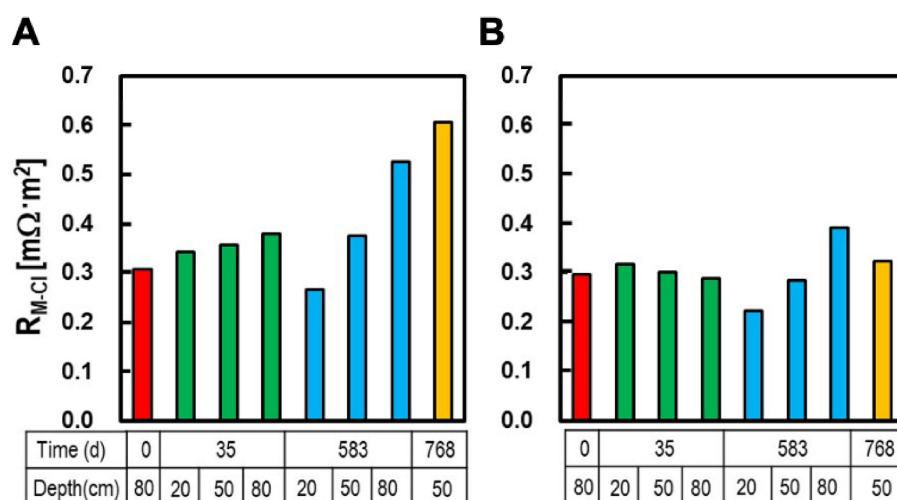


Figure 4. Effect of AEM age on cathode reaction in an H<sub>2</sub>-oxidizing air-cathode fuel cell filled with sewage wastewater as anolyte.

### 3.5. Membrane Resistance in NaCl Solution

The AEM resistance measured in terms of the Cl<sup>−</sup> mobility in the 0.5 M NaCl solution. In this experiment, AEMs were taken from the MFC<sub>AEM</sub> after operation times of 35, 583, and 768 d at depths of 20, 50, and 80 cm (Table 2 and Figure 5).





**Figure 5.** Membrane resistance ( $R_{M-Cl}$ ) as  $Cl^{-}$  mobility of AEMs taken from different depths and operation times. Panels (A,B) indicate  $R_{M-Cl}$  of the AEMs after 1 h and 6 weeks of immersion in 0.5 M NaCl, respectively.

The membrane resistance ( $R_{M-Cl}$ ) of the original AEM was  $0.31 \text{ m}\Omega \cdot \text{m}^2$ , which increased to 0.36, 0.37, and  $0.61 \text{ m}\Omega \cdot \text{m}^2$  in the  $MFC_{AEM}$  at a depth of 50 cm after 35, 583, and 768 d, respectively.  $R_{M-Cl}$  also tended to increase with increasing depth. For instance, for the  $MFC_{AEM}$  at 583 d, the  $R_{M-Cl}$  was  $0.27 \text{ m}\Omega \cdot \text{m}^2$  at 20 cm, and it increased by 1.4 and 2.0 times at depths of 50 cm and 80 cm, respectively. This trend was also observed in the  $MFC_{AEM}$  at 35 d, but the depth-dependent rate of increase was less than that at 583 d. After six weeks of AEM immersion in 0.5 M of NaCl, the surface dirt peeled off from the AEM, which resulted in a 97–110% recovery of  $R_{M-Cl}$  compared to the original  $R_{M-Cl}$  of  $AEM_0$ . This indicates that the surface dirt caused a significant increase in  $R_{M-Cl}$ , in contrast to the marginal increase resulting from the irreversible damage caused to the membrane.

### 3.6. Investigation of Dirt on Membrane

Ion chromatograph analysis of white precipitates on the cathode side of the AEM and CEM revealed the presence of  $Ca^{2+}$ ,  $Mg^{2+}$ , and  $Na^{+}$  as cations for both membranes (Supplementary Figure S2). The AEMs obtained from the MFC operated for 583 d exhibited 0.21, 0.11, and  $0.0037 \text{ mg/cm}^2$  of  $Ca^{2+}$ ,  $Mg^{2+}$ , and  $Na^{+}$ , respectively. It is hypothesized that the cations are transferred from wastewater and through the AEM by the extreme water pressure. The CEM at 35 d exhibited 0.29, 0.019, and  $0.047 \text{ mg/cm}^2$  for  $Ca^{2+}$ ,  $Mg^{2+}$ , and  $Na^{+}$ , respectively.  $Cl^{-}$  was detected as an anion because 0.1 M of HCl was used as the solvent for both membranes. In contrast, the anode side of the AEM and CEM exhibited an apparent increase in microbial density (Supplementary Figure S3). These results indicate that Ca, Mg, and Na salts that are eluted from wastewater appear as precipitates on the cathode side and that microbial biofilm appears as the brown dirt on the anode side.

## 4. Conclusions

The comparison of air-cathode MFC performances equipped with the AEM and CEM indicated the superiority of the AEM as a separator. The use of AEMs reduced the cathode resistance by eliminating the pH imbalance observed in an air-cathode MFC equipped with a CEM. Moreover, the AEM showed an increase in membrane resistance as the  $Cl^{-}$  mobility with the increase in operation time and depth. This result indicates a potential increase in membrane resistance when using the AEM in large-scale MFCs at the meter scale for extended periods. However, the increase in membrane resistance marginally contributes to the cathode resistance with  $OH^{-}$  movement for less than 768 d and at a depth of less than 1 m.

**Supplementary Materials:** The following supporting information can be downloaded at: <https://www.mdpi.com/article/10.3390/membranes12020183/s1>, Figure S1: The illustration and apparatus of the reactor used for the LSV experiment; Figure S2: Identified ions precipitated on the cathode side of ion-exchange membranes in MFCs; Figure S3: Fluorescence microscopic images of microbes attached to the AEMs before MFC installation and 583 d after the operation.

**Author Contributions:** R.I., data curation and writing—original draft preparation; N.Y., writing—review and editing, supervision, project administration, funding acquisition; T.Y., data curation; Y.K., data curation; M.H., supervision. All authors have read and agreed to the published version of the manuscript.

**Funding:** This study was supported by JST A-step (Grant number: JPMJTM20EK), the MILT Sewage Applied Research Program, and the JSPS Joint Research Program with NSFC and was partially supported by Nippon Koei Co., Ltd. and Tamano Consultants Co., Ltd.

**Informed Consent Statement:** Not applicable.

**Acknowledgments:** We would like to thank Kazuki Iida and Hiroaki Kobayashi from Nippon Koei Co., Ltd. for coordinating the research collaboration, Mitsuhiro Sakoda and Akihiro Iwata from Tamano Consultants Co., Ltd. for their kind support in the reactor construction, and Takahiro Matsumura from TOYOBO Co., Ltd. for manufacturing the MFC core. We also thank the staff of the Nagoya City Waterworks and Sewerage Bureau for providing access to the test sites and advisory comments.

**Conflicts of Interest:** The authors declare no conflict of interest.

## References

1. UNESCO. *The United Nations World Water Development Report 2021 Valuing Water*; UNESCO: Paris, France, 2021; ISBN 9789231004346.
2. Sugioka, M.; Yoshida, N.; Iida, K. On Site Evaluation of a Tubular Microbial Fuel Cell Using an Anion Exchange Membrane for Sewage Water Treatment. *Front. Energy Res.* **2019**, *7*, 91. [[CrossRef](#)]
3. Lu, M.; Chen, S.; Babanova, S.; Phadke, S.; Salvacion, M.; Mirhosseini, A.; Chan, S.; Carpenter, K.; Cortese, R.; Bretschger, O. Long-term performance of a 20-L continuous flow microbial fuel cell for treatment of brewery wastewater. *J. Power Source* **2017**, *356*, 274–287. [[CrossRef](#)]
4. Jin, P.; Gu, Y.; Shi, X.; Yang, W. Non-negligible greenhouse gases from urban sewer system. *Biotechnol. Biofuels* **2019**, *12*, 100. [[CrossRef](#)] [[PubMed](#)]
5. Franz, M. Phosphate fertilizer from sewage sludge ash (SSA). *Waste Manag.* **2008**, *28*, 1809–1818. [[CrossRef](#)]
6. McCarty, P.L.; Bae, J.; Kim, J. Domestic wastewater treatment as a net energy producer—can this be achieved? *Environ. Sci. Technol.* **2011**, *45*, 7100–7106. [[CrossRef](#)]
7. Logan, B.E.; Hamelers, B.; Rozendal, R.; Schröder, U.; Keller, J.; Freguia, S.; Aelterman, P.; Verstraete, W.; Rabaey, K. Microbial fuel cells: Methodology and technology. *Environ. Sci. Technol.* **2006**, *40*, 5181–5192. [[CrossRef](#)]
8. AlSayed, A.; Soliman, M.; Eldyasti, A. Microbial fuel cells for municipal wastewater treatment: From technology fundamentals to full-scale development. *Renew. Sustain. Energy Rev.* **2020**, *134*, 110367. [[CrossRef](#)]
9. Liu, H.; Logan, B.E. Electricity generation using an air-cathode single chamber microbial fuel cell in the presence and absence of a proton exchange membrane. *Environ. Sci. Technol.* **2004**, *38*, 4040–4046. [[CrossRef](#)]
10. Nojavan, S.; Zare, K.; Mohammadi-Ivatloo, B. Application of fuel cell and electrolyzer as hydrogen energy storage system in energy management of electricity energy retailer in the presence of the renewable energy sources and plug-in electric vehicles. *Energy Convers. Manag.* **2017**, *136*, 404–417. [[CrossRef](#)]
11. Zhang, H.; Sun, C. Cost-effective iron-based aqueous redox flow batteries for large-scale energy storage application: A review. *J. Power Source* **2021**, *493*, 229445. [[CrossRef](#)]
12. Dong, Y.; Qu, Y.; He, W.; Du, Y.; Liu, J.; Han, X.; Feng, Y. A 90-liter stackable baffled microbial fuel cell for brewery wastewater treatment based on energy self-sufficient mode. *Bioresour. Technol.* **2015**, *195*, 66–72. [[CrossRef](#)] [[PubMed](#)]
13. Hiegemann, H.; Littfinski, T.; Krimmler, S.; Lübken, M.; Klein, D.; Schmelz, K.G.; Ooms, K.; Pant, D.; Wichern, M. Performance and inorganic fouling of a submersible 255 L prototype microbial fuel cell module during continuous long-term operation with real municipal wastewater under practical conditions. *Bioresour. Technol.* **2019**, *294*, 122227. [[CrossRef](#)]
14. Goto, Y.; Yoshida, N. Scaling up Microbial Fuel Cells for Treating. *Water* **2019**, *11*, 1803. [[CrossRef](#)]
15. Rossi, R.; Jones, D.; Myung, J.; Zikmund, E.; Yang, W.; Gallego, Y.A.; Pant, D.; Evans, P.J.; Page, M.A.; Cropek, D.M.; et al. Evaluating a multi-panel air cathode through electrochemical and biotic tests. *Water Res.* **2019**, *148*, 51–59. [[CrossRef](#)]
16. Cheng, S.; Liu, H.; Logan, B.E. Increased performance of single-chamber microbial fuel cells using an improved cathode structure. *Electrochem. Commun.* **2006**, *8*, 489–494. [[CrossRef](#)]
17. Al Lawati, M.J.; Jafary, T.; Baawain, M.S.; Al-Mamun, A. A mini review on biofouling on air cathode of single chamber microbial fuel cell; prevention and mitigation strategies. *Biocatal. Agric. Biotechnol.* **2019**, *22*, 101370. [[CrossRef](#)]

18. Liu, W.; Cheng, S.; Yin, L.; Sun, Y.; Yu, L. Influence of soluble microbial products on the long-term stability of air cathodes in microbial fuel cells. *Electrochim. Acta* **2018**, *261*, 557–564. [[CrossRef](#)]
19. Pasternak, G.; Greenman, J.; Ieropoulos, I. Regeneration of the power performance of cathodes affected by biofouling. *Appl. Energy* **2016**, *173*, 431–437. [[CrossRef](#)] [[PubMed](#)]
20. Ge, Z.; He, Z. Long-term performance of a 200 liter modularized microbial fuel cell system treating municipal wastewater: Treatment, energy, and cost. *Environ. Sci. Water Res. Technol.* **2016**, *2*, 274–281. [[CrossRef](#)]
21. Ge, Z.; Wu, L.; Zhang, F.; He, Z. Energy extraction from a large-scale microbial fuel cell system treating municipal wastewater. *J. Power Source* **2015**, *297*, 260–264. [[CrossRef](#)]
22. Sugioka, M.; Yoshida, N.; Yamane, T.; Kakihana, Y.; Higa, M.; Matsumura, T.; Sakoda, M.; Iida, K. Long-term evaluation of an air-cathode microbial fuel cell with anion exchange membrane in a 226 L wastewater treatment reactor. *Environ. Res.* **2022**, *205*, 112416. [[CrossRef](#)] [[PubMed](#)]
23. Rossi, R.; Wang, X.; Logan, B.E. High performance flow through microbial fuel cells with anion exchange membrane. *J. Power Source* **2020**, *475*, 228633. [[CrossRef](#)]
24. Rossi, R.; Baek, G.; Saikaly, P.E.; Logan, B.E. Continuous Flow Microbial Flow Cell with an Anion Exchange Membrane for Treating Low Conductivity and Poorly Buffered Wastewater. *ACS Sustain. Chem. Eng.* **2021**, *9*, 2946–2954. [[CrossRef](#)]
25. Rossi, R.; Logan, B.E. Using an anion exchange membrane for effective hydroxide ion transport enables high power densities in microbial fuel cells. *Chem. Eng. J.* **2021**, *422*, 130150. [[CrossRef](#)]
26. Yamane, T.; Yoshida, N.; Sugioka, M. Estimation of total energy requirement for sewage treatment by a microbial fuel cell with a one-meter air-cathode assuming Michaelis–Menten COD degradation. *RSC Adv.* **2021**, *11*, 20036–20045. [[CrossRef](#)]
27. Feng, Y.; Yang, Q.; Wang, X.; Logan, B.E. Treatment of carbon fiber brush anodes for improving power generation in air-cathode microbial fuel cells. *J. Power Source* **2010**, *195*, 1841–1844. [[CrossRef](#)]
28. Yoshida, N.; Miyata, Y.; Iida, K. Current recovery from sewage wastewater using electrochemically oxidized graphite felt. *RSC Adv.* **2019**, *9*, 39348–39354. [[CrossRef](#)]
29. Goto, Y.; Yoshida, N.; Umeyama, Y.; Yamada, T.; Tero, R.; Hiraishi, A. Enhancement of Electricity Production by Graphene Oxide in Soil Microbial Fuel Cells and Plant Microbial Fuel Cells. *Front. Bioeng. Biotechnol.* **2015**, *3*, 42. [[CrossRef](#)]
30. Rossi, R.; Cario, B.P.; Santoro, C.; Yang, W.; Saikaly, P.E.; Logan, B.E. Evaluation of Electrode and Solution Area-Based Resistances Enables Quantitative Comparisons of Factors Impacting Microbial Fuel Cell Performance. *Environ. Sci. Technol.* **2019**, *53*, 3977–3986. [[CrossRef](#)] [[PubMed](#)]
31. Fujii, K.; Yoshida, N.; Miyazaki, K. Michaelis–Menten equation considering flow velocity reveals how microbial fuel cell fluid design affects electricity recovery from sewage wastewater. *Bioelectrochemistry* **2021**, *140*, 107821. [[CrossRef](#)]
32. Mehdizadeh, S.; Yasukawa, M.; Abo, T.; Kakihana, Y.; Higa, M. Effect of spacer geometry on membrane and solution compartment resistances in reverse electrodialysis. *J. Memb. Sci.* **2019**, *572*, 271–280. [[CrossRef](#)]
33. Goto, Y.; Yoshida, N. Microbially reduced graphene oxide shows efficient electricity recovery from artificial dialysis wastewater. *J. Gen. Appl. Microbiol.* **2017**, *63*, 165–171. [[CrossRef](#)] [[PubMed](#)]
34. Yoshida, N.; Miyata, Y.; Mugita, A.; Iida, K. Electricity recovery from municipal sewage wastewater using a hydrogel complex composed of microbially reduced graphene oxide and sludge. *Materials* **2016**, *9*, 742. [[CrossRef](#)] [[PubMed](#)]
35. Logan, B.; Cheng, S.; Watson, V.; Estadt, G. Graphite fiber brush anodes for increased power production in air-cathode microbial fuel cells. *Environ. Sci. Technol.* **2007**, *41*, 3341–3346. [[CrossRef](#)]
36. Nagahashi, W.; Yoshida, N. Comparative evaluation of fibrous carbons and bamboo charcoal in the recovery of current from sewage wastewater. *J. Gen. Appl. Microbiol.* **2021**, *67*, 248–255. [[CrossRef](#)] [[PubMed](#)]
37. Lanas, V.; Ahn, Y.; Logan, B.E. Effects of carbon brush anode size and loading on microbial fuel cell performance in batch and continuous mode. *J. Power Source* **2014**, *247*, 228–234. [[CrossRef](#)]